Article:
Zhao, H., Wynne, B.P. and Palmiere, E.J. (2016) A phase quantification method based on EBSD data for a continuously cooled microalloyed steel. Materials Characterization, 123. pp. 339-348. ISSN: 1044-5803

https://doi.org/10.1016/j.matchar.2016.11.024

Accepted Manuscript

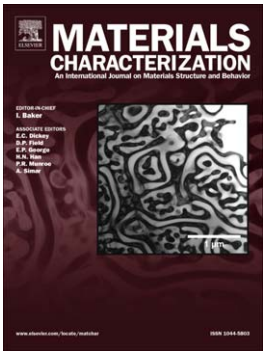

A phase quantification method based on EBSD data for a continuously cooled microalloyed steel

Haitao Zhao, Eric J Palmiere, Bradley P Wynne

PII: S1044-5803(16)30972-X
DOI: doi: 10.1016/j.matchar.2016.11.024
Reference: MTL 8464

To appear in: *Materials Characterization*

Received date: 1 September 2016
Revised date: 14 November 2016
Accepted date: 16 November 2016

Please cite this article as: Zhao Haitao, Palmiere Eric J, Wynne Bradley P, A phase quantification method based on EBSD data for a continuously cooled microalloyed steel, *Materials Characterization* (2016), doi: 10.1016/j.matchar.2016.11.024

A phase quantification method based on EBSD data for a continuously cooled microalloyed steel

Haitao Zhao, Eric J Palmiere, Bradley P Wynne

Department of Materials Science and Engineering, The University of Sheffield, Sir Robert Hadfield Building, Mappin Street, Sheffield, S1 3JD, UK

Corresponding author：Haitao Zhao，tel: +44 (0) 114 222 5978，email：mtp12hz@sheffield.ac.uk

Keywords: Phase quantification; Acicular ferrite; Bainitic ferrite; Microalloyed steel; Electron backscatter diffraction

Abstract:

Mechanical properties of steels depend on the phase constitutions of the final microstructures which can be related to the processing parameters. Therefore, accurate quantification of different phases is necessary to investigate the relationships between processing parameters, final microstructures and mechanical properties. Point counting on micrographs observed by optical or scanning electron microscopy is widely used as a phase quantification method, and different phases are discriminated according to their morphological characteristics. However, it is difficult to differentiate some of the phase constituents with similar morphology. Differently, for EBSD based phase quantification methods, besides morphological characteristics, other parameters derived from the orientation information can also be used for discrimination. In this research, a phase quantification method based on EBSD

data in the unit of grains was proposed to identify and quantify the complex phase constitutions of a microalloyed steel subjected to accelerated coolings. Characteristics of polygonal ferrite/quasi-polygonal ferrite, acicular ferrite and bainitic ferrite on grain averaged misorientation angles, aspect ratios, high angle grain boundary fractions and grain sizes were analysed and used to develop the identification criteria for each phase. Comparing the results obtained by this EBSD based method and point counting, it was found that this EBSD based method can provide accurate and reliable phase quantification results for microstructures with relatively slow cooling rates.

1. Introduction

Microalloyed steels subjected to accelerated cooling no longer have microstructures of ferrite and pearlite but show microstructures composed of various austenite decomposition products [1]. According to the classification systems proposed by Araki et al. [2] and Krauss et al. [3], ferritic transformation products can be divided into several categories including polygonal ferrite (PF), quasi-polygonal ferrite (QF), granular bainite (GB), acicular ferrite (AF) and lath bainite (LB).

PF and QF are reconstructive transformation products. PF forms at the slowest cooling rates and the highest transformation temperatures. It nucleates at austenite grain boundaries and grows into an equiaxed shape [3]. QF often forms in very-low-carbon steels under rapid cooling [4]. In this condition, single-phase austenite can transform into single-phase ferrite without a composition change, and the QF grains formed are usually coarse and have irregular and jagged grain boundaries [3].

At low transformation temperatures, GB and LB transformations become dominant [5, 6]. GB packets form at relatively higher temperatures and mainly consist of wide parallel laths. The boundaries between GB laths are usually low angle grain boundaries (LAGBs) with small misorientation angles [7] and are difficult to be revealed by orientation sensitive etchants like nital [8]. Therefore, it is difficult to observe these lath boundaries and only the packet boundaries can be revealed clearly [9], which makes GB packets looks like grains with an almost entirely granular aspect [10]. Differently, LB packets form at relatively lower temperatures and consist of fine parallel laths [11]. Some of these lath boundaries are high angle grain boundaries (HAGBs) with misorientation angles higher than 15° and are prone to be revealed by etching with nital. Therefore, areas with a clear lath-like morphology correspond to LB microstructures [9]. Despite the difference in morphology, GB is not different from LB in terms of the transformation mechanism, and both of them mainly consist of parallel laths and contain a high density of dislocations [10]. Therefore, in this research, both GB and LB are termed as bainitic ferrite (BF).

In microalloyed steels, acicular ferrite (AF) was defined as a highly substructured, non-equiaxed ferrite that forms on continuous cooling [12]. It consists of laths with a chaotic and irregular arrangement [10]. In optical micrographs, adjacent AF laths sometimes form packets, which have a veined appearance [12, 13] and many boundary protrusions [14]. Despite the unique morphology of AF, many research results indicate that AF shows a similar transformation behaviour to that of BF [15-18].

Based on the description above, each transformation product (phase) has its specific transformation mechanism, morphology and substructures. Mechanical properties of steels

depend on the phase constitutions of the final microstructures which can be related to the processing parameters. Therefore, accurate quantification of different phases is necessary to investigate the relationships between processing parameters, final microstructures and mechanical properties [19].

In order to get the area fractions of different phases, various techniques are available. The most frequently used is point counting on micrographs observed by optical microscopy (OM) or scanning electron microscopy (SEM). Different phases are discriminated based on their morphological characteristics. However, it was found in research [9] that some grains with the same morphology belong to different phases and it is very difficult to differentiate QF grains from GB packets using OM or SEM. Therefore, the phase quantification results obtained by point counting inevitably differ from person to person [19]. Differently, various EBSD based phase quantification methods have been proposed and most of them can be divided into two groups, methods in the unit of pixels (measured points) and those in the unit of grains.

According to the phase transformation characteristics of steels, phases transformed at different temperatures have different defect densities [10]. Those phases formed at lower temperatures, such as AF, BF and martensite, normally have a higher density of dislocations which lead to degraded electron backscatter patterns (EBSPs) and high orientation gradients. Therefore, phase quantification methods in the unit of pixels can be further divided into two sub-groups, one using quantitative measurements of EBSP clarity [19] and the other one taking advantage of the crystallographic information of EBSD mapping to reveal orientation gradients.

To quantify EBSP clarity, various parameters have been used, such as image quality (IQ), band slope (BS) and confidence index (CI). IQ values describe the average intensity of the

Kikuchi bands with respect to the overall intensity within the pattern [19]. BS values are the gradients of maximum intensity changes between the Kikuchi bands and the pattern background [20]. CI values are the quantitative measurements of the reliability of EBSP indexing [21]. IQ and BS are derived from the Hough transformation of EBSPs and CI is calculated during the indexing of EBSPs [20]. These parameters have been effectively used for phase quantification in dual phase steels [9, 19, 22-24] and multiphase steels [19, 20, 24, 25].

Besides the limited data obtained directly from each pixel, derivative information can also be generated because the coordinates of each measured point are also recorded during EBSD mapping [19]. Orientation gradient is a typical derived value and has been used for phase quantification in a TRIP steel [26]. It was found in that research that among all pixel-based values, only orientation gradient allows reliable separation of BF from PF.

Although these quantification methods in the unit of pixels sometimes provide good matches with the point counting results, they do suffer from some drawbacks. For the methods based on EBSP clarity, besides defect densities, pattern clarity also depends on grain orientations [20], contaminations [26], sample preparation methods [20], and even surface topology [19]. In some cases, possibly due to the use of high-resolution FEG–SEM which delivers good EBSPs, neither CI nor IQ profiles exhibit separated peaks that allow clear phase separation [20, 26]. Therefore, all of these EBSP clarity values are susceptible to external factors and sometimes their influences can be overwhelming. Another factor that influences the phase quantification results is grain boundaries. Due to the EBSP overlap of neighbouring grains, pixels near grain boundaries also have low pattern clarity, which could make these pixels be mistakenly identified as BF or martensite [21, 26]. Therefore, for quantification

methods based on EBSP clarity, grain boundary related pixels should be excluded [24]. Lastly, using methods in the unit of pixels, pixels within the same grain are frequently identified as different phases, which is unreasonable from a metallurgical perspective [9, 19].

To overcome these drawbacks, phase quantification methods in the unit of grains were proposed [9, 19, 27]. These grain-based methods effectively avoid the problem that pixels within the same grain are identified as different phases. To detect grains from EBSD data, boundaries with misorientation angles higher than a threshold value can be shown and blocks of pixels enclosed by these boundaries can be regarded as grains defined by this misorientation angle threshold value.

The key feature of these grain-based methods is using various grain-related or grain-averaged properties for phase discrimination. A range of direct or derived information of pixels inside a grain can be averaged such as values of IQ, BS, CI and orientation gradient [19]. In research [22] grain-averaged BS values were used to separate bainite from ferrite and martensite and grain-average IQ values were adopted to differentiate ferrite from martensite. In research [19], grain-averaged BS and IQ values were used together to discriminate martensite from bainite and ferrite. However, due to the same reason as illustrated above for the methods in the unit of pixels, values of IQ, BS and CI are susceptible to external factors, and the influence of external factors will be carried through the grain averaging process, which makes the phase quantification result unreliable. Derived values, like orientation gradients, can also be grain-averaged. Grain-averaged misorientation (GAM) angles calculated by averaging the intra-granular misorientation angles between neighbouring pixels can be regarded as grain-averaged orientation gradients [19]. In addition, after grain detection, many grain-related

morphological parameters can also be obtained, such as grain size, aspect ratio and grain boundary misorientation. Using both grain-averaged values and grain-related morphological parameters, accurate phase quantification results can be obtained [9, 19, 28].

In this research, a phase quantification method based on EBSD data in the unit of grains were proposed for a continuously cooled microalloyed steel. Samples of a niobium microalloyed steel were subjected to different combinations of thermomechanical processing and continuous cooling to get various transformation microstructures. Theses microstructures were exploited to develop the identification criteria for each phase, and both grain-averaged values and grain-related morphological parameters were used to identify and quantify the area fractions of PF/QF, AF and BF.

2. Experimental

To simulate the industrial rolling process, plane strain compression (PSC) tests were adopted and conducted on a 0.045C-1.43Mn-0.14Si-0.09Nb-0.21Cr-0.12Ni-0.21Cu-0.01Ti steel. The processing route is illustrated in Figure 1. Samples were reheated to 1200˚C at a rate of 10˚C/s, held for 2 minutes for equilibration, and then cooled at a rate of 5˚C/s to 1100˚C for a roughing deformation (strain1) of 0.3 at a constant true strain rate of $10s^{-1}$. Following roughing, samples were cooled immediately to 950˚C at a rate of 5˚C/s for the second deformation with strain2. This second deformation was also performed at a constant true strain rate of $10s^{-1}$, and was followed by an accelerated cooling from 950˚C to 500˚C at various cooling rates between 5~50˚C/s, a slow cooling from 500˚C to 350˚C at a rate of 1˚C/s, and finally a water quenching from 350˚C to room temperature.

To get final microstructures with different phase constitutions and subsequently use these microstructures to develop the phase identification criteria, various strain2 volumes and continuous cooling rates were adopted in this research. The strain2 volumes, cooling rates and corresponding sample names are shown in Table 1. Another sample subjected to the same processing profile but water quenched directly to room temperature before strain2 was used as a reference material in Section 4.2.

Specimens for metallographic observation were cut in the rolling direction–normal direction (RD-ND) plane, and were ground and polished carefully. To reveal the transformed microstructures, a 2% nital solution was used as an etchant and the microstructures were examined under JEOL JSM-6400 SEM. To prepare specimens particularly for EBSD mapping, after grinding and polishing, specimens were polished with a colloidal silica suspension for additional 2 minutes. EBSD mapping was performed in the RD-ND plane of specimens on a FEI Sirion FEG-SEM with a step size of 0.2 μm and accelerating voltage of 20 kV. The diffraction patterns were collected using an Oxford Instrument Nordlys CCD Camera with HKL Channel 5 Flamenco package. Subsequently obtained data were processed and analysed using HKL Channel 5 post-processing package and an in-house program. To reduce the mis-indexing of phases in these complex microstructures, α iron was chosen as the only matching unit.

3. Transformed microstructures

3.1 Microstructures under SEM

SEM secondary electron micrographs of the transformed microstructures of samples A, B, C and D with various strain2 volumes and cooling rates are shown in Figure 2.

In Figure 2 (a), the parallel morphology of the transformation product can be seen clearly. Prior austenite grain boundaries (PAGBs) remain, and the parallel laths developed from the PAGBs extended into the austenite grains, sometimes even across the whole grain, which is typical BF morphology. In Figure 2 (b) and (c), with strain2 of 0.5, non-equiaxed lathes with an irregular and chaotic arrangement become the dominant phase which can be classified as AF. Together with these irregular AF laths are some BF packets of parallel laths in both microstructures. Additionally, for sample B with the relatively slow cooling rate, 5˚C/s, equiaxed PF/QF grains can be found in the microstructure, Figure 2 (b). Despite strain2 of 0.5, increasing the cooling rate further to 50˚C/s, BF packets of parallel laths become the dominant phase together with some irregular AF laths, Figure 2(d). Throughout all the micrographs, fine martensite/austenite (M/A) constituents can be found distributed within the matrix, appearing white under SEM. The formation of this microphase can be attributed to the partitioning of carbon from ferrite laths to austenite during transformation [29]. Therefore, by altering the strain2 volumes and the cooling rates, microstructures with different phase constitutions were obtained successfully.

3.2 EBSD mapping

Following the noise reduction procedures illustrated in Section 4.1, a small area of each EBSD data set was used to plot an inverse pole figure (IPF) coloured orientation map and a corresponding boundary map as shown in Figure 3 (a)~(d) and Figure 3 (e)~(h) respectively. For phase quantification, each whole data set was used. We can see that each microstructure has its distinct characteristics of morphology and boundary misorientation angles. These characteristics were illustrated together with the development of phase discrimination criteria in Section 4.

4. Phase identification criteria

4.1 Noise reduction and grain detection

Prior to phase quantification, filtration of raw EBSD data and definition of structural units should be done. Filtration of raw EBSD data includes correcting mis-indexed points and filling non-indexed points. Non-indexed points can be related to the existence of M/A constituents and grain boundaries. In research [28], non-indexed points due to the existence of martensite were separated from those at grain boundaries and were used to evaluate the area fraction of martensite. However, in this research, some of the M/A constituents are found distributed at grain boundaries, which make the separation difficult and unreliable. Differently, as shown in research [9, 26], M/A constituents can be revealed by etching with tint etchants and also can be reliably quantified by point counting. It is not necessary to quantify the area fraction of M/A constituents through EBSD based techniques. Therefore, in this research, following a

recommended method [30], mis-indexed points of raw data were removed and non-indexed points were filled with the common orientations of their neighbours using Channel 5 post-processing software.

For phase quantification methods in the unit of grains, a grain detection misorientation angle (GDMA) should be set to define the grain units. In research [9, 22, 26], 1.5˚ or 2˚ were chosen to define grains, while higher angles, 3˚ or 5˚, were selected in investigations [19, 27]. However, another factor needs to consider is the angular resolution of an EBSD system. For normal EBSD systems, the angular resolution is around 1˚ [31, 32]. Therefore the GDMA should be higher than 2˚ and it was found that low GDMAs like 1.5˚ often lead to abnormal fragmentation of a single grain [19]. Furthermore, GDMAs of 1.5˚ or 2˚ were mainly chosen to separate PF/QF grains from BF laths nucleated on them in TRIP steels with high fractions of PF/QF [26]. While in microalloyed steels, PF/QF transformations are usually suppressed by accelerated coolings to guarantee the strength level. However, the GDMA should not be so high that different phases are included in a single grain. Therefore, a medium GDMA of 5˚ was used to detect grains in this research.

Usually after grain detection, there are still artefacts in the form of tiny grains with just several pixels [27]. The formation of these tiny grains may be related to the remaining mis-indexed points. To remove these tiny grains, i.e. the remaining mis-indexed points, a critical grain area need to be selected. Since the existence of these tiny grains can be revealed by the spikes on an aspect ratio distribution curve [27], as shown in Figure 4 (a) for sample B, the critical grain area can be selected as the lowest value which make the spikes on the aspect ratio distribution curve disappear by removing grains smaller than it. For sample B, the critical

grain area was identified as 1.2 μm^2 and after removing the grains with areas lower than 1.2 μm^2, the aspect ratio distribution curve appears smooth as shown in Figure 4 (b). Very similar changes were also observed in other samples. Therefore, after grain detection, a further noise reduction was conducted by removing the tiny grains with areas lower than 1.2 μm^2, and only the grains left were selected for the following phase quantification procedures.

4.2 Identification of reconstructive phases

Due to the similar transformation mechanisms of AF and BF, it is easier to differentiate PF/QF from AF and BF at first. Since PF/QF grains are evident in sample B, the criteria to identify PF/QF grains were developed based on the EBSD data of sample B.

PF and QF both are reconstructive transformation products and form at higher temperatures. Therefore the defect densities of PF and QF are lower than those of AF and BF, which results in the lower GAM angles of PF/QF grains. This is evident in Figure 3 (f) where LAGBs are seldom found in some of the equiaxed grains. Accordingly, the GAM distribution curve of sample B shown in Figure 5 is asymmetrical, which indicates that more than one phases with their unique GAM angle distributions contribute to the overall GAM profile. Since PF/QF and AF/BF have different defect densities and thus distinct GAM distributions, the overall GAM curve was disassociated into two peaks as shown by the dashed lines in Figure 5, the peak with lower GAM angles representing PF/QF while the other one representing AF/BF. It is clear from the GAM peak of PF/QF shown in Figure 5 that the majority of PF/QF grains have GAM angles lower than 3°, which is consistent with the result in research [27]. Furthermore, careful examination of the PF/QF grains in different microstructures reveals that

most of them have GAM angles smaller than 3˚. But in research [9], a much smaller GAM threshold value, 1.5˚, was chosen. This discrepancy is related to the difference in the grain definition misorientation angle (GDMA). Besides defect densities, GAM angles are also influenced by the grain size and thus the GDMA [27]. The smaller the GDMA, the finer the grain sizes, and the smaller the overall GAM angles. In research [9], a smaller GDMA, 2˚, was used, leading to the lower GAM threshold value.

This grain size dependent characteristic of GAM angles also brings about another problem worth considering. That is when the size of a grain is below a critical value, no matter it is a reconstructive or a displacive transformation product, it will have a low GAM angle. Therefore, GAM angles can only be used for phase identification for those grains with sizes above this critical value. To identify this value, the water quenched sample with bainite/martensite microstructure shown in Figure 6 was used as a reference material. It is clear in Figure 6 that bainite/martensite laths or plates nucleated on PAGBs and extended into austenite grains, which makes PAGBs remain. Therefore, the existence of PF/QF microstructures in this water quenched sample can be ruled out.

The relationships between the mean GAM angles and the grain sizes for this water quenched sample and sample B are shown in Figure 7 and Figure 8 respectively. It should be noted that in this research grain sizes are represented by grain areas which are obtained by the multiplication of the quantity of EBSD data points within each grain and the area of a single data point, 0.04 μm^2. In Figure 7 (a) and (b), we can see that both the mean GAM angles and their standard deviations generally decrease with the reduction of the grain area. In Figure 7 (c) and (d), only the mean GAM angles of the small grains (grain areas $\leq$ 40 μm^2) and their

standard deviations are shown. It is clear that for grains with areas no greater than 10 μm^2, most of their mean GAM angles are lower than 2˚ and the standard deviations are lower than 1˚, which indicates that for these small grains, most of their GAM angles are below 3˚ even when they are bainite or martensite grains. A similar relationship between the mean GAM angle, the standard deviation and the grain area can also be observed for sample B as shown in Figure 8. Therefore, GAM angles can only be used as a criterion for those grains with areas larger than 10 μm^2. This is another reason why small GDMAs were not used in this research, because small GDMAs can result in small grain sizes, leading to the invalidity of the GAM angle as a criterion.

Inevitably, AF/BF grains with areas above 10 μm^2 may also have GAM angles lower than 3˚. Therefore, aspect ratios and grain boundary misorientation characteristics were used to refine the results. The aspect ratio distribution for sample B shown in Figure 4 (b) is also asymmetrical as the GAM curve shown in Figure 5. Therefore, this aspect ratio curve can be disassociated into several peaks with unique aspect ratio distributions. In Figure 2(b) and Figure 3(f), we can see that PF/QF grains usually have equiaxed shapes, namely low aspect ratios, while most of the AF laths tend to have high aspect ratios as shown in Figure 2(c) and Figure 3(g). As for the aspect ratio of BF, since adjacent BF laths usually have similar orientations [10], the BF grains defined by the GDMA of 5˚ consist of several BF laths. Although BF laths usually have high aspect ratios to reduce the transformation strain energy [10], the aspect ratios of BF grains are scattered in a wide range and depend on the quantity and arrangement of BF laths within each BF grain [27]. Based on the characteristics illustrated above, the aspect ratio distribution curve in Figure 4 was disassociated into two peaks as shown

by the dashed lines, the peak with lower aspect ratios representing PF/QF while the other one representing AF. It is clear from the PF/QF peak shown in Figure 4 that the majority of PF/QF grains have aspect ratios lower than 2. As for the grain boundary misorientation characteristic, it is evident in Figure 3(f) that most of the equiaxed grains are surrounded by HAGBs. Therefore, for grains with areas larger than 10 μm^2 and GAM angles lower than 3°, those ones with aspect ratios below 2 and HAGB fractions higher than 0.9 were identified as PF/QF. Here the HAGB fraction of each grain is the length fraction of HAGBs within all the boundaries of this grain.

For grains with areas no greater than 10 μm^2, aspect ratio and grain boundary misorientation characteristic can be used to identify the PF/QF grains among them. Therefore, PF/QF grains can be selected by the criteria shown in Table 2.

4.3 Differentiation of AF from BF

After the identification of PF/QF grains, the remaining grains were subjected to the following procedures to discriminate AF from BF. The criteria to identify AF grains were developed based on the EBSD data of samples B and C because AF is the dominant microstructure for these samples. Since AF and BF have similar transformation mechanisms and the defect densities of AF and BF are very close as indicated by the significant overlap of IQ peaks of AF and BF [24, 33], GAM angles of AF and BF should also overlap a lot. Therefore, other parameters are necessary for a precise discrimination of AF from BF.

Despite the similar transformation mechanisms, the fundamental difference between AF and BF is that AF laths nucleate intragranularly at austenite deformation substructures while

BF laths primarily nucleate on austenite grain boundaries [34-36]. BF nucleated on PAGBs finally develops into packets of parallel laths. During BF transformation, strong variant selection occurs and under relatively slow cooling rates or high transformation temperatures, variant selection mainly favours the variant pairs with low misorientation angles [37], resulting in the low density of HAGBs and the large grain size of BF. But for AF, the formation of laths nucleated directly at intragranular nucleation sites can weaken the variant selection mechanism, so that more types of variants and variant pairs are generated in each austenite grain [38, 39]. Furthermore, AF does not develop into packets of parallel laths on a large scale because the development of packets is prohibited by the impingement between adjacently nucleated AF laths [10]. Actually, several adjacent parallel AF laths form packets on a small scale and different AF packets have different lengthening directions [15]. AF packets will impinge with others formed at nearby nucleation sites, which prevents the formation of overall parallel morphology and brings about the irregular and chaotic morphology of AF [15].

Based on the differences between AF and BF, AF grains can be identified by the following two steps. Firstly, a grain area threshold value was identified and grains with sizes smaller than this value were selected. To get this grain area threshold value, the relationships between grain areas and area fractions for samples B and C are shown in Figure 9. A clear bimodal distribution of the area fraction with respect to the grain area can be seen in Figure 9 (a) and (b). Since AF grains usually have small grain areas and large quantities, Figure 3 (b) and (c), within each grain area bin there are a large number of grains and the quantity of grains within each bin decreases with the rise of the grain area. These characteristics of AF grains result in a generally continuous area fraction distribution and a downward trend with the rise of the grain area. On

the other hand, BF grains usually have large grain areas and relatively small quantities, which leave only one or two grains within each grain area bin. These characteristics of BF grains lead to a scattered area fraction distribution and an upward trend with the increased grain area. Therefore, the grain area threshold value can be identified at the valley point where the overall trend changes from downward to upward with the increased grain area. As shown in Figure 9 (c) and (d), the valley points can be identified clearly. For consistency and easy comparison, the same grain area threshold value, 70 μm^2, was adopted in this research and grains with areas below this value were selected.

Then, among these selected small grains, those grains with HAGB fractions higher than 0.5 were identified as AF. The reason why a HAGB fraction threshold value of 0.5 was selected is illustrated below. After the grain detection, some small-sized BF laths bounded by LAGBs with misorientation angles higher than 5˚ but lower than 15˚ can be found within BF packets. Without the restriction on HAGB fractions, these small-sized BF laths can be mistakenly identified as AF. While in some AF lath packets, the existence of boundaries with misorientation angles higher than 5˚ but lower than 15˚ between AF laths can split an AF lath packet bounded by HAGBs into two grains each with a HAGB fraction higher than 0.5. Using a large HAGB fraction threshold value (e.g. 0.9 for PF/QF grains) will exclude these grains from AF grains. Therefore, an intermediate HAGB fraction threshold value, 0.5, was selected. In summary, after the identification of PF/QF grains, the remaining grains with areas smaller than 70 μm^2 and HAGB fractions higher than 0.5 can be identified as AF grains. BF grains can be discriminated by difference after the identification of PF/QF and AF. Based on the discussion above, the criteria used to identify AF are summarised in Table 2.

5. Phase quantification results and discussion

Phase constitutions of samples A, B, C and D have been quantified by point counting on multiple SEM micrographs to obtain reference values of phase area fractions. The quantification results are shown in Table 3.

Differently, according to the criteria listed in Table 2, the phase quantification results of samples A, B, C and D based on the EBSD data are shown in Table 4. Although criteria should be specific for each sample, here the same criteria were adopted for different samples to keep consistency and validate comparison.

By comparing the results in Table 3 and Table 4, it is evident that the differences in the phase quantification results of samples A, B, and C are relatively small, especially in the AF area fractions. But for sample D, there is an evident discrepancy and the reason for that can be explained below. For the EBSD based phase quantification method proposed in this research, the separation of AF and BF is based on the assumption that BF transforms at relatively slow cooling rates or high temperatures at which variant selections favour laths with small misorientation angles within packets as shown in Figure 3 (e), (f) and (g), with cooling rates of 20, 5 and 20˚C/s, respectively. Due to this variant selection, BF packets identified under SEM usually have large grain areas and can be readily identified by the EBSD based method in this research. But increasing the cooling rate further to 50˚C/s, sample D, laths with rather large misorientation angles will be favoured in BF packets to self-accommodate the transformation strain [37] as shown in Figure 3 (h). Under this condition, BF packets identified under SEM may consist of several grains with small grain areas and large HAGB fractions, and thus be

mistakenly identified as AF grains by the EBSD based method. Therefore, the EBSD based phase quantification method proposed in this research is only reliable for samples subjected to relatively slow accelerated coolings.

It is also evident that there are relatively large differences in the area fractions of PF/QF for all samples, and the area fractions of BF are also influenced because they were determined by difference after the quantification of PF/QF and AF and the results of AF fractions are very close except for sample D. The reason why fractions of PF/QF are underestimated during point counting is that judging only by morphological characteristics is difficult to differentiate PF/QF grains from BF packets after etching with nital [9]. Since nital is an orientation sensitive etchant [8] and BF laths within a packet usually have similar orientations, especially under slow cooling rates, BF lath boundaries within a packet may not be revealed very well after etching with nital, which makes some BF packets appear equiaxed and featureless. The similarity of morphology between BF and PF/QF can easily make the phase quantification by point counting biased. While for the method based on EBSD data, besides morphological characteristics, other objective criteria were used to assure the accuracy of PF/QF quantification. Therefore, the EBSD based quantification method proposed in this research can provide accurate and reliable results for microstructures composed of complex phases with relatively slow cooling rates.

6. Conclusion

In this research, a phase quantification method based on EBSD data in the unit of grains was proposed to identify and quantify the complex phase constitutions of a microalloyed steel

subjected to accelerated coolings. The characteristics of PF/QF, AF and BF on grain averaged misorientation (GAM) angles, aspect ratios, high angle grain boundary (HAGB) fractions and grain sizes were analysed and used to develop the identification criteria for each phase. PF/QF grains usually have equiaxed shapes, low defect densities and HAGBs. Therefore, those grains with aspect ratios smaller than 2, GAM angles lower than 3˚ and HAGB fractions higher than 0.9 were identified as PF/QF. Since it was found that GAM angles are only valid for grains with areas larger than 10 μm^2, these criteria were only applied to the grains with areas larger than 10 μm^2. For the grains with areas no greater than 10 μm^2, only the criteria on aspect ratios and HAGB fractions were used to identify PF/QF. As for AF, its characteristics of small grain areas and relatively high densities of HAGBs were used to set the criteria. Valley points of the area fraction distributions were used to obtain the grain area threshold value, 70 μm^2. Those grains with areas smaller than 70 μm^2 and HAGB fractions higher than 0.5 were selected as AF. Finally, the area fraction of BF was obtained by difference. Comparing the results obtained by this EBSD based method and point counting, it was found that this EBSD based method can provide accurate and reliable phase quantification results for microstructures with relatively slow cooling rates.

Acknowledgements

This work was supported by Companhia Brasileira de Metalurgia e Mineração (CBMM) and China Scholarship Council (CSC).

Reference

[1] I. Takeuchi, et al., The prospects for high-grade steel pipes for gas pipelines, Pipes and Pipelines International, 48 (2003) 33-43.

[2] T. Araki, et al., Atlas for Bainitic microstructures, ISIJ, Tokyo, Japan, 1992.

[3] G. Krauss, S.W. Thompson, Ferritic microstructures in continuously cooled low-and ultralow-carbon steels, ISIJ international, 35 (1995) 937-45.

[4] G. Krauss, Steels: processing, structure, and performance, ASM International, Materials Park, Ohio, 2005.

[5] D. Tian, et al., Correlation between microstructural features of granular bainite, roughness of fracture surface and toughness of simulated CGHAZ in QT type HSLA steels, Scandinavian Journal of Metallurgy, 25 (1996) 87-94.

[6] H.J. Jun, et al., Effects of deformation and boron on microstructure and continuous cooling transformation in low carbon HSLA steels, Materials Science and Engineering: A, 422 (2006) 157-62.

[7] A. Lambert-Perlade, et al., Austenite to bainite phase transformation in the heat-affected zone of a high strength low alloy steel, Acta Materialia, 52 (2004) 2337-48.

[8] G.F. Vander Voort, Metallography, principles and practice, ASM International, Materials Park, Ohio, 1984.

[9] K. Zhu, et al., Characterization and quantification methods of complex BCC matrix microstructures in advanced high strength steels, Journal of Materials Science, 48 (2013) 413-23.

[10] H.K.D.H. Bhadeshia, Bainite in steels, Institute of Materials, London, 1992.

[11] M. Smirnov, et al., Classification of low-carbon pipe steel microstructures, Metallurgist, 54 (2010) 444-54.

[12] Y. Smith, et al., Manganese-Molybdenum-Niobium Acicular Ferrite Steels with High Strength and Toughness, Toward improved ductility and toughness, Climax Molybdenum Company (Japan) Ltd, Kyoto, 1972, pp. 119-42.

[13] J.L. Lee, et al., The intermediate transformation of Mn-Mo-Nb steel during continuous cooling, Journal of Materials Science, 22 (1987) 2767-77.

[14] L. Collins, et al., Microstructures of linepipe steels, Canadian Metallurgical Quarterly, 22 (1983) 169-79.

[15] Z. Tang, W. Stumpf, The role of molybdenum additions and prior deformation on acicular ferrite formation in microalloyed Nb–Ti low-carbon line-pipe steels, Materials Characterization, 59 (2008) 717-28.

[16] Y.M. Kim, et al., Effects of molybdenum and vanadium addition on tensile and charpy impact properties of API X70 linepipe steels, Metallurgical and Materials Transactions A, 38 (2007) 1731-42.

[17] S. Lee, et al., Transformation strengthening by thermomechanical treatments in C-Mn-Ni-Nb steels, Metallurgical and Materials Transactions A, 26 (1995) 1093-100.

[18] Y.M. Kim, et al., Transformation behavior and microstructural characteristics of acicular ferrite in linepipe steels, Materials Science and Engineering A, 478 (2008) 361-70.

[19] J.-Y. Kang, et al., Phase analysis of steels by grain-averaged EBSD functions, ISIJ international, 51 (2011) 130-6.

[20] E.P. Kwon, et al., Characterization of transformed and deformed microstructures in transformation induced plasticity steels using electron backscattering diffraction, Materials Science and Engineering: A, 528 (2011) 5007-17.

[21] R. Petrov, et al., Microstructure and texture of a lightly deformed TRIP-assisted steel characterized by means of the EBSD technique, Materials Science and Engineering: A, 447 (2007) 285-97.

[22] L. Ryde, Application of EBSD to analysis of microstructures in commercial steels, Materials Science and Technology, 22 (2006) 1297-306.

[23] A. Wilson, et al., Determining phase volume fraction in steels by electron backscattered diffraction, Scripta materialia, 45 (2001) 1335-40.

[24] J. Wu, et al., Image quality analysis: a new method of characterizing microstructures, ISIJ international, 45 (2005) 254-62.

[25] M. De Meyer, et al., Texture development in cold rolled and annealed C-Mn-Si and C-Mn-Al-Si TRIP steels, Materials science and technology, 17 (2001) 1353-9.

[26] S. Zaefferer, et al., EBSD as a tool to identify and quantify bainite and ferrite in low - alloyed Al - TRIP steels, Journal of Microscopy, 230 (2008) 499-508.

[27] S.L. Shrestha, et al., An automated method of quantifying ferrite microstructures using electron backscatter diffraction (EBSD) data, Ultramicroscopy, 137 (2014) 40-7.

[28] J.-Y. Kang, et al., Estimation of phase fraction in dual phase steel using microscopic characterizations and dilatometric analysis, Materials Characterization, 84 (2013) 205-15.

[29] M.C. Zhao, et al., Continuous cooling transformation of undeformed and deformed low carbon pipeline steels, Materials Science and Engineering: A, 355 (2003) 126-36.

[30] L. Sun, et al., Mapping microstructure inhomogeneity using electron backscatter diffraction in 316L stainless steel subjected to hot plane strain compression tests, Materials Science and Technology, 26 (2010) 1477-86.

[31] N.C. Krieger Lassen, The relative precision of crystal orientations measured from electron backscattering patterns, Journal of Microscopy, 181 (1996) 72-81.

[32] V. Randle, Microtexture determination and its applications, The Institute of Materials, London, 1992.

[33] A. J. DeArdo, et al., New method of characterizing and quantifying complex microstructures in steels, Materials and Manufacturing Processes, 25 (2010) 33-40.

[34] C. Chiou, et al., The effect of prior compressive deformation of austenite on toughness property in an ultra-low carbon bainitic steel, Materials chemistry and physics, 69 (2001) 113-24.

[35] S. Yamamoto, et al., Effects of the austenite grain size and deformation in the unrecrystallized austenite region on bainite transformation behavior and microstructure, ISIJ international, 35 (1995) 1020-6.

[36] J. Yang, et al., The influence of plastic deformation and cooling rates on the microstructural constituents of an ultra-low carbon bainitic steel, ISIJ international, 35 (1995) 1013-9.

[37] N. Takayama, et al., Effects of transformation temperature on variant pairing of bainitic ferrite in low carbon steel, Acta Materialia, 60 (2012) 2387-96.

[38] M. Díaz-Fuentes, I. Gutiérrez, Analysis of different acicular ferrite microstructures generated in a medium-carbon molybdenum steel, Materials Science and Engineering A, 363 (2003) 316-24.

[39] A.-F. Gourgues, et al., Electron backscattering diffraction study of acicular ferrite, bainite, and martensite steel microstructures, Materials Science and Technology, 16 (2000) 26-40.

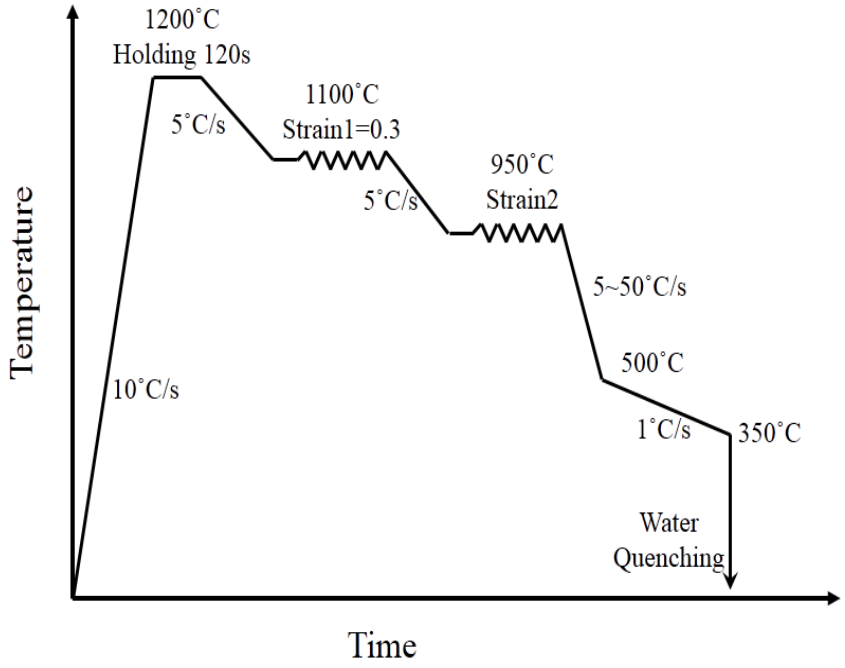

Figure 1

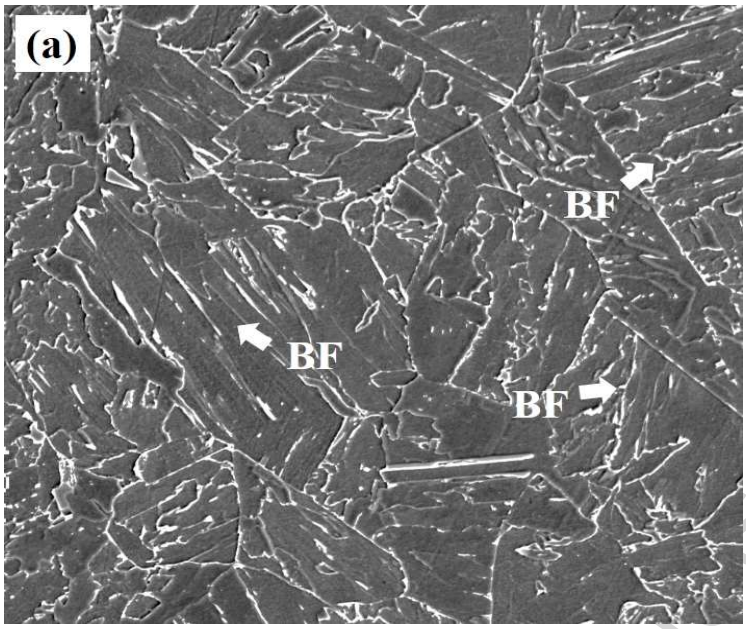

Figure 2a

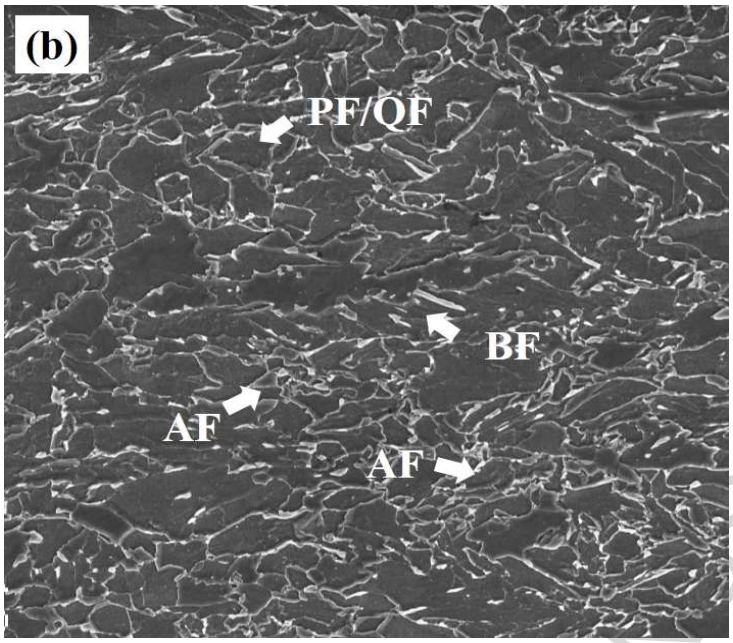

Figure 2b

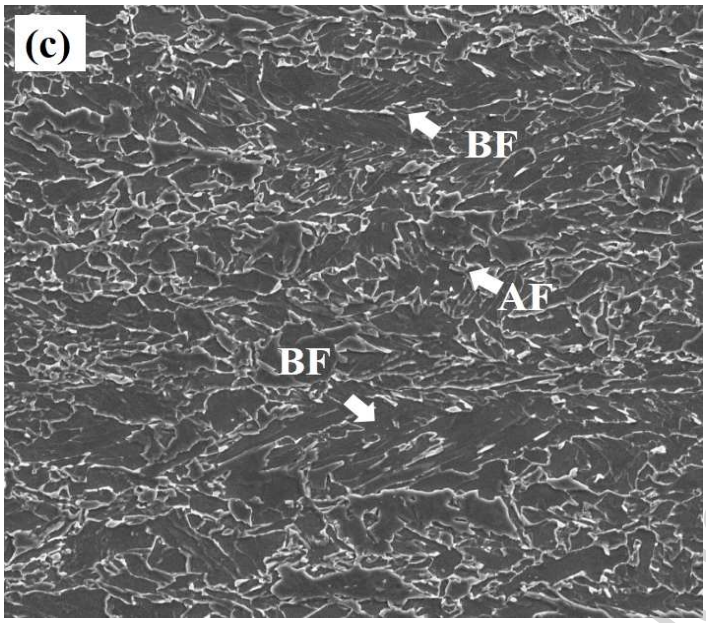

Figure 2c

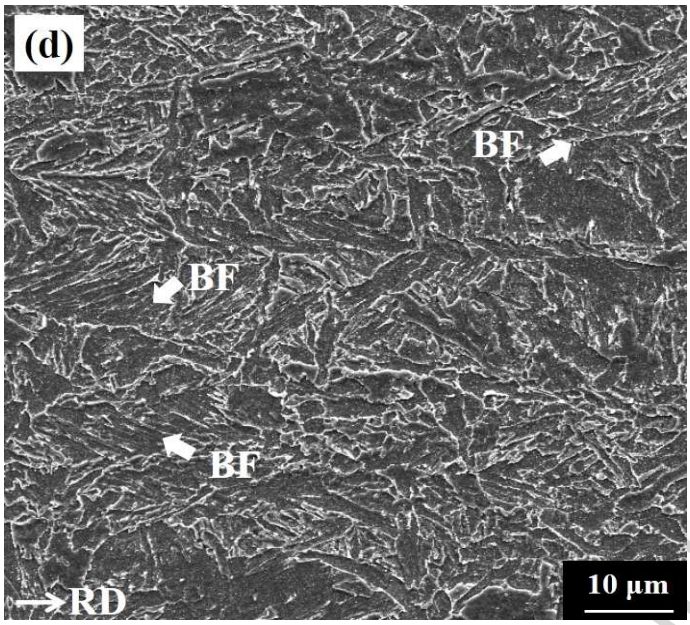

Figure 2d

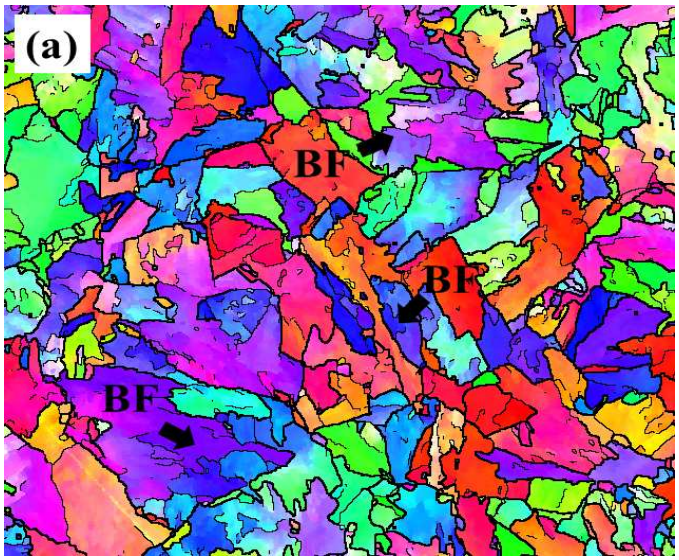

Figure 3a

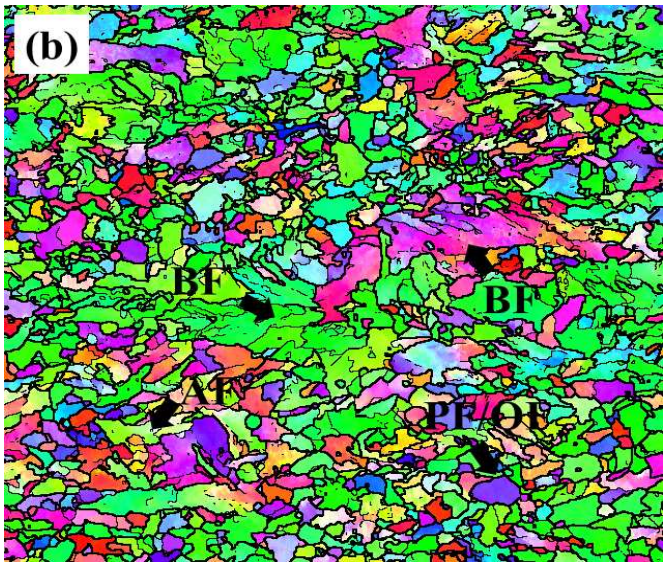

Figure 3b

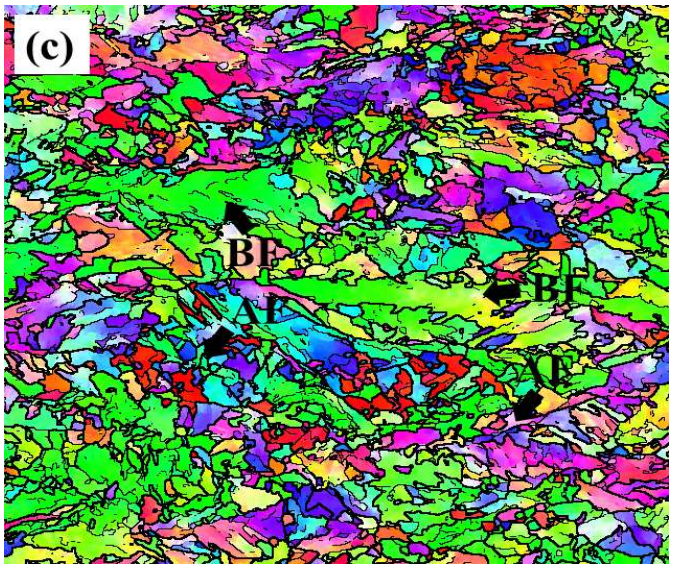

Figure 3c

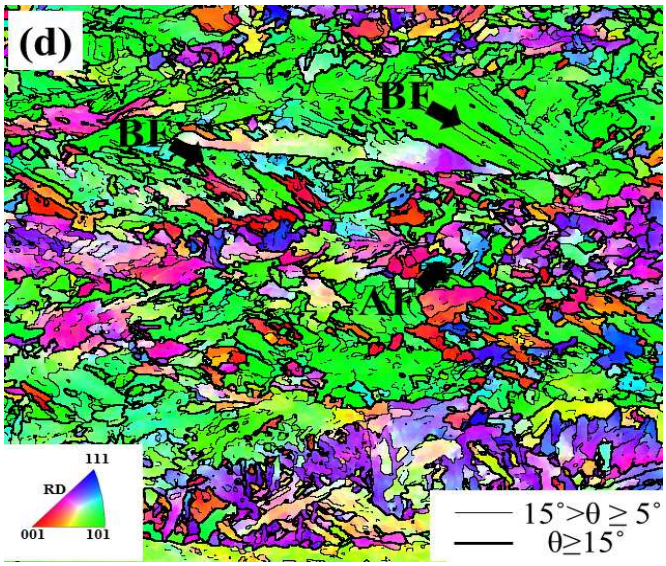

Figure 3d

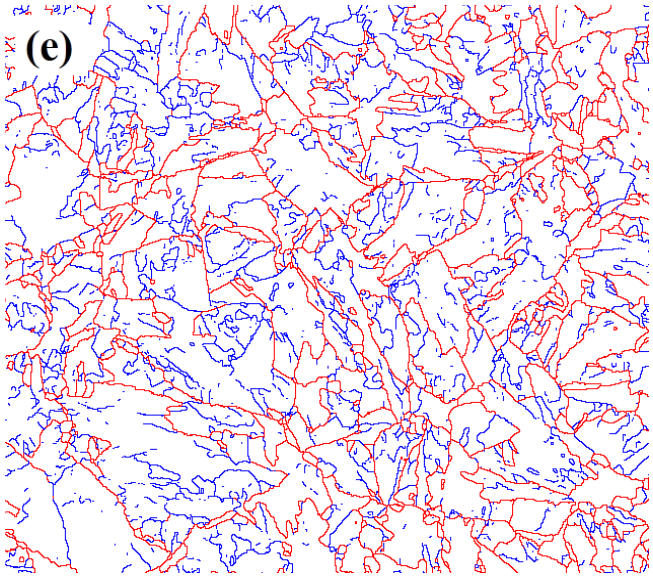

Figure 3e

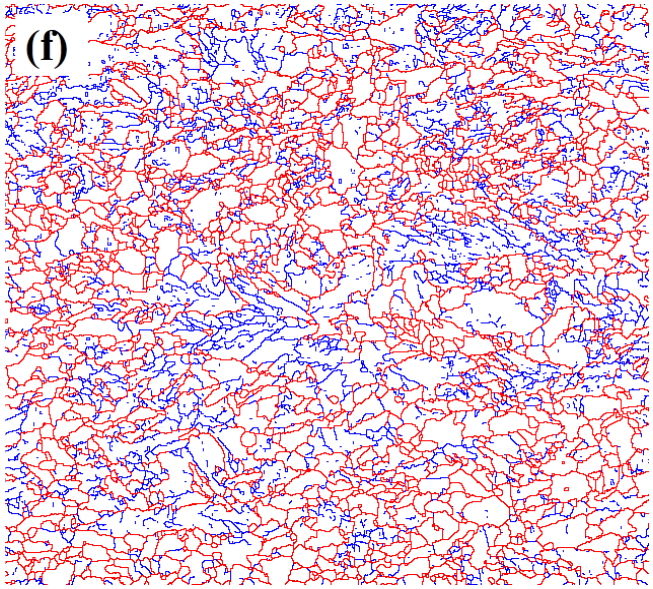

Figure 3f

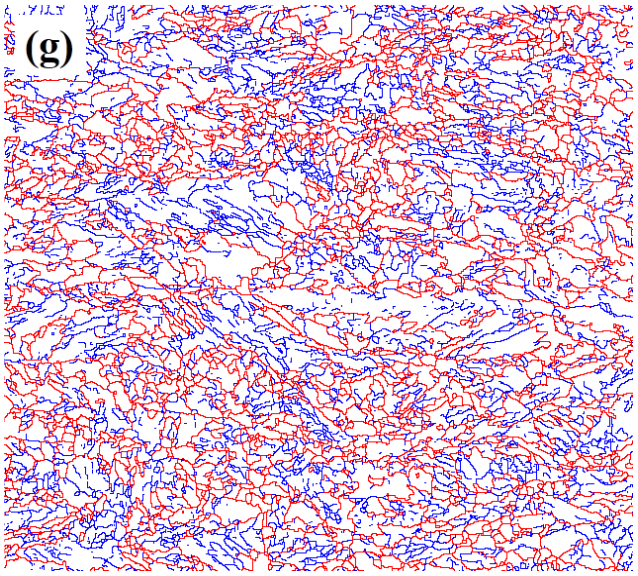

Figure 3g

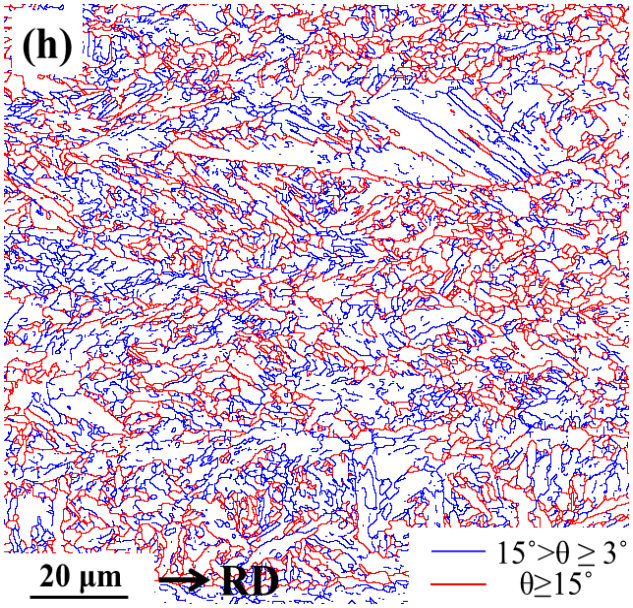

Figure 3h

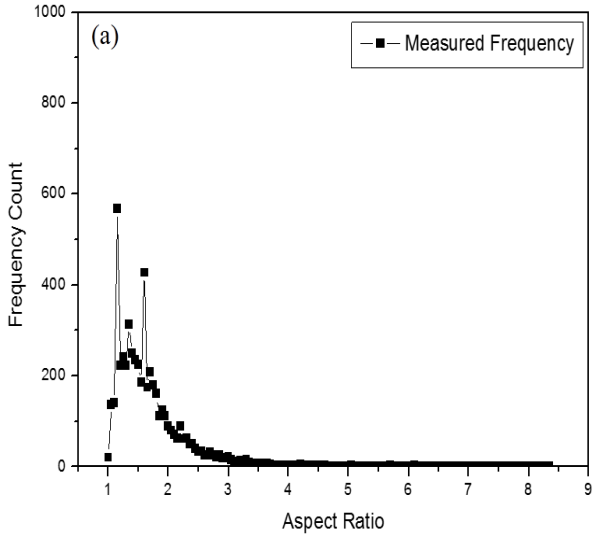

Figure 4a

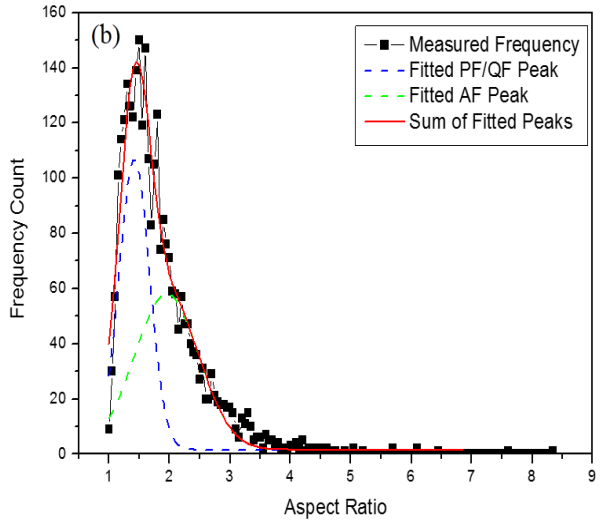

Figure 4b

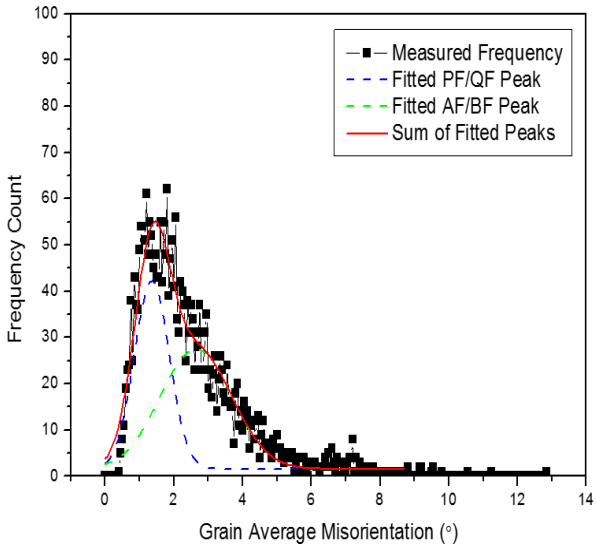

Figure 5

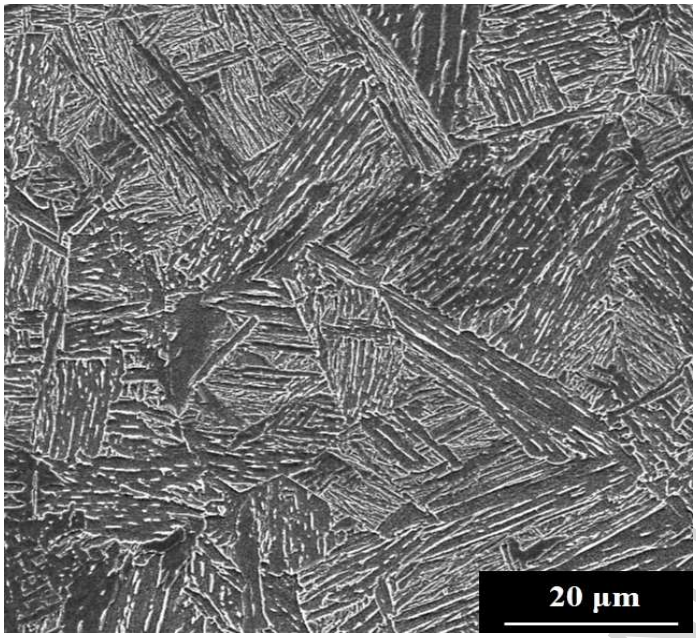

Figure 6

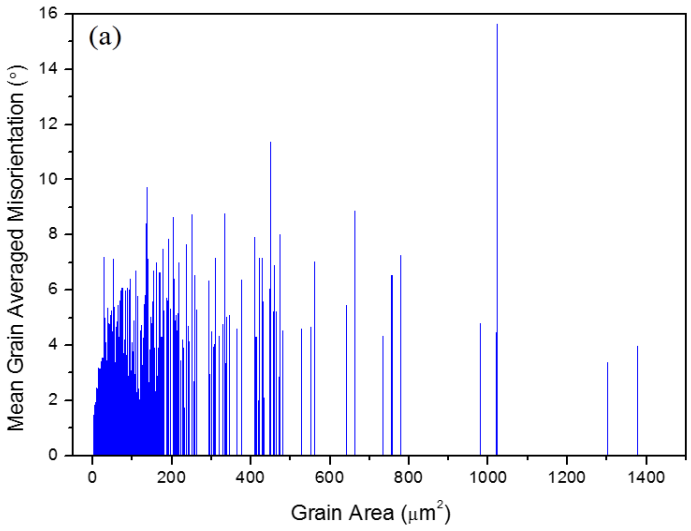

Figure 7a

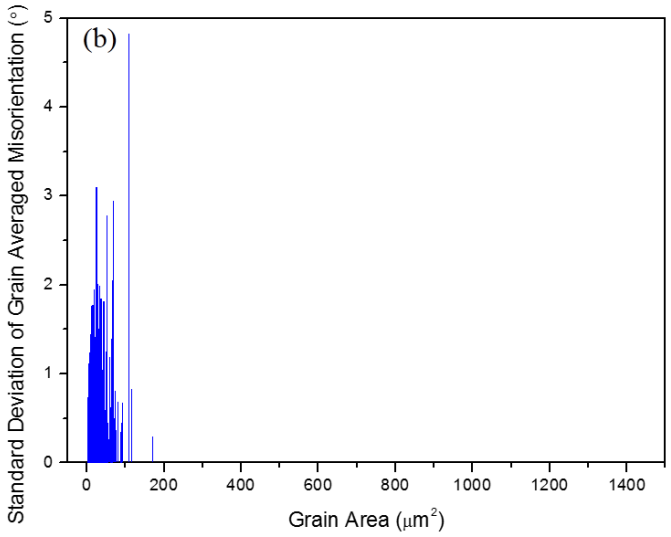

Figure 7b

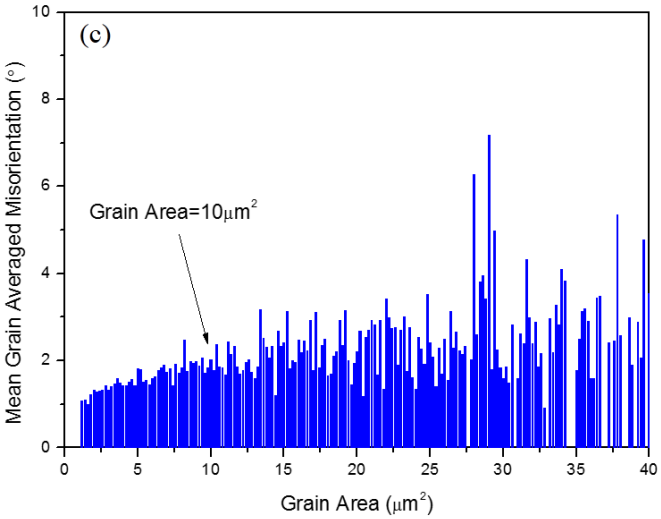

Figure 7c

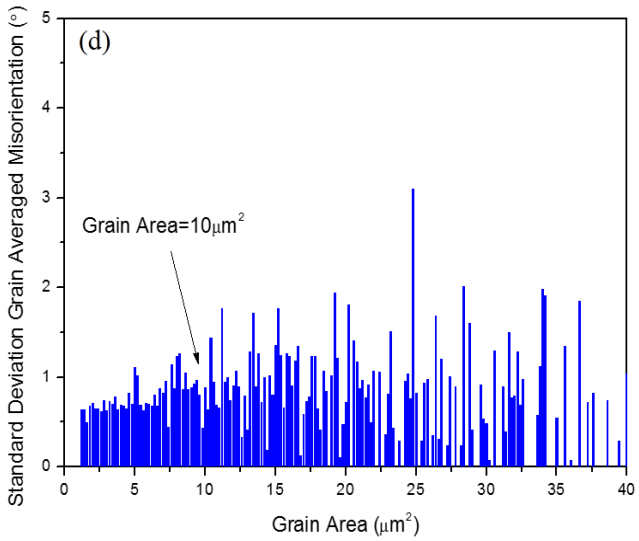

Figure 7d

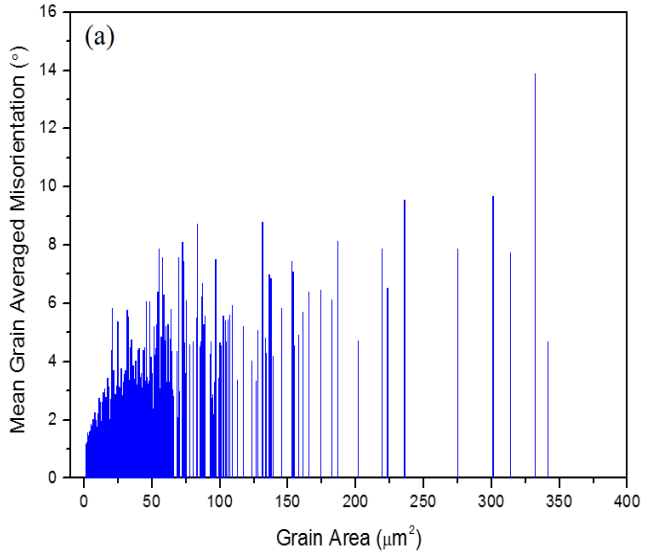

Figure 8a

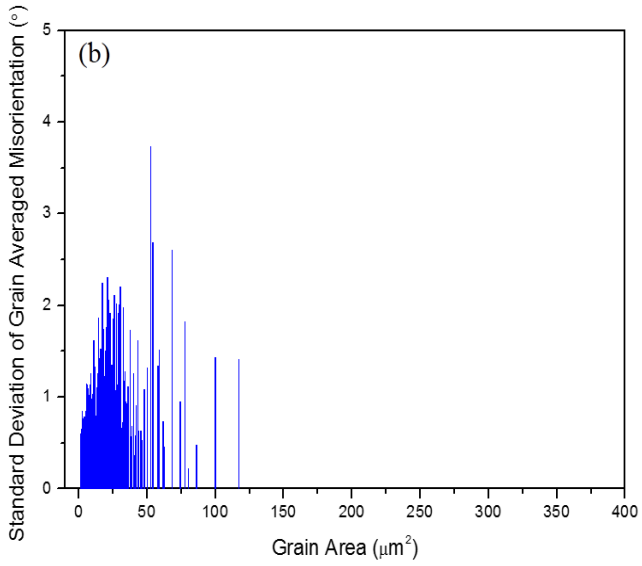

Figure 8b

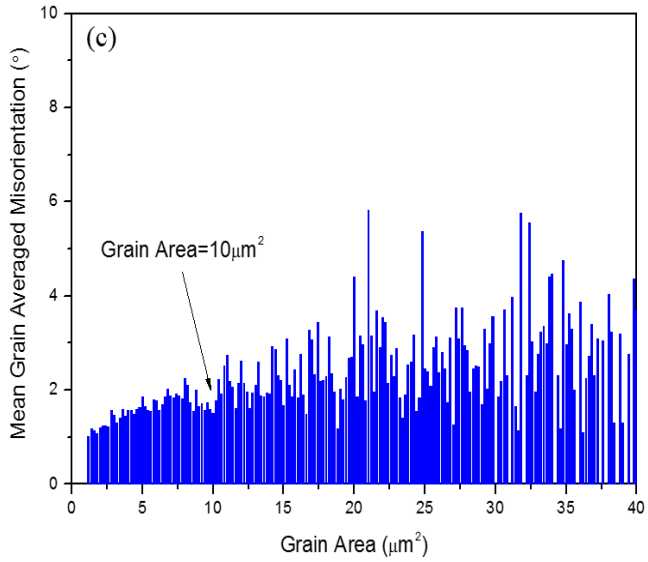

Figure 8c

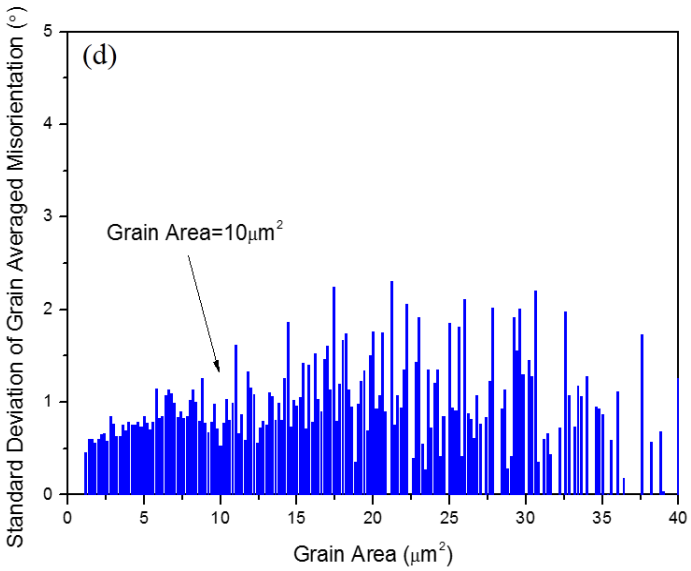

Figure 8d

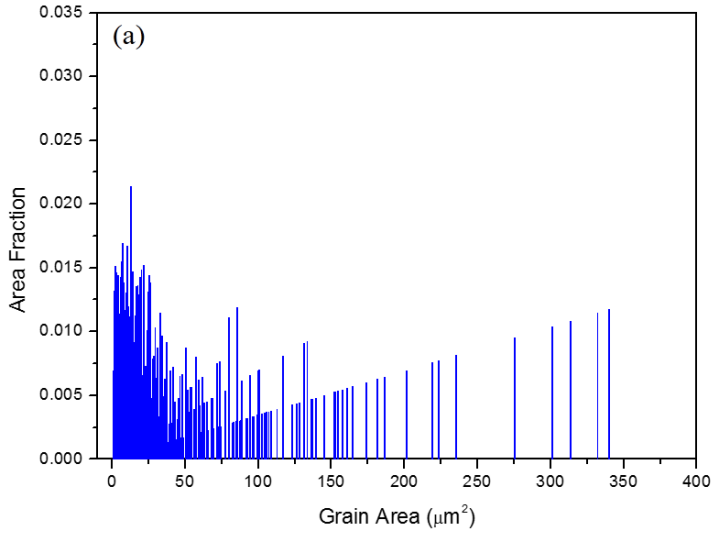

Figure 9a

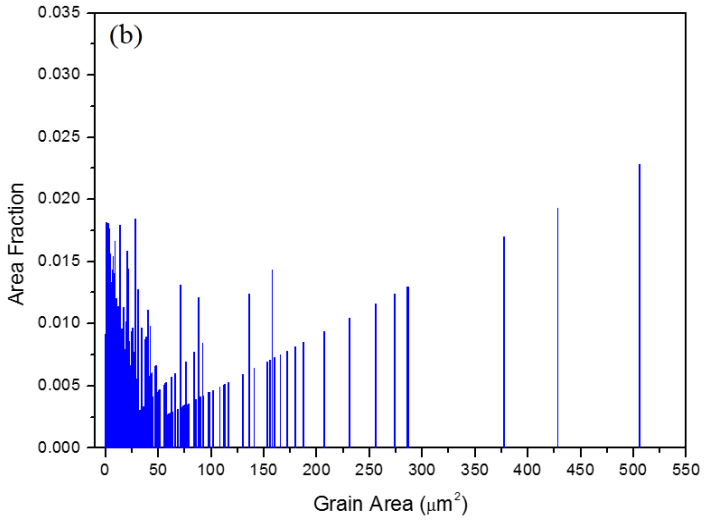

Figure 9b

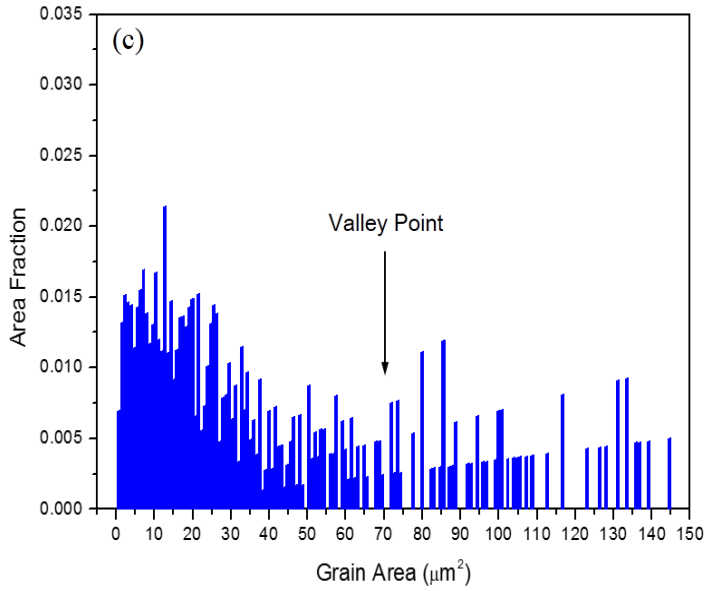

Figure 9c

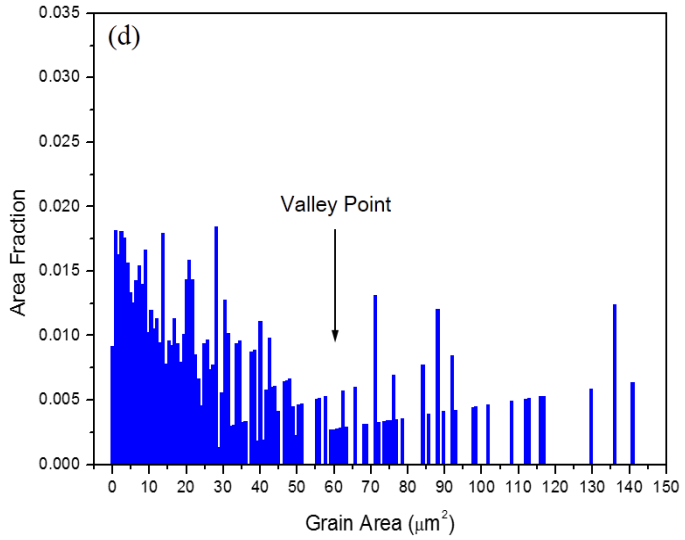

Figure 9d

Table 1 Austenite deformation volume and cooling rate for each sample.

Sample name	A	B	C	D
Strain2 volume	0	0.5	0.5	0.5
Cooling rate (˚C/s)	20	5	20	50

Table 2 Criteria for the identification of PF/QF, AF and BF.

Phase	Aspect ratio	Grain boundary characteristic	Grain averaged misorientation	Grain area
PF/QF	<2	HAGB fraction>0.9	<3˚	>10 μm^2
	<2	HAGB fraction>0.9	—	≤10 μm^2
AF	—	HAGB fraction>0.5	—	<70 μm^2
BF	—	—	—	—

Table 3 Area fractions obtained by point counting.

Sample name	A	B	C	D
PF/QF	0.02	0.13	0.04	0.01
AF	0.18	0.48	0.59	0.25
BF	0.80	0.39	0.37	0.74

Table 4 Area fractions obtained by the EBSD based method proposed.

Sample name	A	B	C	D
PF/QF	0.09	0.22	0.10	0.07
AF	0.18	0.49	0.52	0.42
BF	0.73	0.29	0.38	0.51

Highlights

1. A phase quantification method based on EBSD data in the unit of grains was proposed.
2. The critical grain area above which GAM angles are valid parameters was obtained.
3. Grain size and grain boundary misorientation were used to identify acicular ferrite.
4. High cooling rates deteriorate the accuracy of this EBSD based method.